JOURNAL OF THE KOREAN ASTRONOMICAL SOCIETY
36: S117 ~ S124, 2003

POINT SPREAD FUNCTION OF THE SOFT X-RAY TELESCOPE ABOARD YOHKOH

JUNHO SHIN AND TAKASHI SAKURAI
Solar Physics Division, National Astronomical Observatory of Japan
Osawa 2-21-1, Mitaka, Tokyo 181-8588, Japan
E-mail: jshin@solar.mtk.nao.ac.jp

ABSTRACT

Pre-launch calibration data have been analyzed for evaluating the point spread function (PSF) of *Yohkoh* Soft X-ray Telescope (SXT). Especially, it is found crucial that the effect of undersampling should be treated properly. The best fit solution of the SXT PSF, which is modeled by an elliptical Moffat function, has been derived by the comparison with the ground experiment data. In order to examine the off-axis variation of the SXT PSF, we need to define in advance the location of the optical axis on the CCD. According to the previous studies, the off-axis variation of effective area (the vignetting function) may be approximated either by two non-concentric cones or by a cone with some flat distortions. There have been, however, no fully approved representations for the SXT vignetting effect. The effect of the shift of the optical axis from the geometrical center of the telescope is investigated by numerical simulation. It is revealed from our study that the full width at half maximum (FWHM) of the SXT PSF stays nearly constant within an error bound over the central area of the CCD where the solar disk is located.

Key words : Sun: Yohkoh—Sun: SXT—Sun: PSF

I. INTRODUCTION

The Soft X-ray Telescope (SXT) aboard *Yohkoh* (Ogawara et al. 1991) has made great contributions for a decade to the research on three dimensional structures of coronal magnetic fields. Aside from morphological studies, one of the purposes using the SXT images is to study the spatial and temporal variation of many physical quantities and interpret the mechanism of coronal activities. For this reason, it has been emphasized by many scientists that the calibrations on the observed SXT data should be carried out very carefully.

For an astronomical observation using optical instruments, it is expected that the information from an object comes out to be blurred by the imperfectness of the observing system. This pattern of blurring is generally expressed by the point spread function (PSF) of an instrument, which defines the intensity distribution over the image of a point source at infinity. An astronomical image is, as a result, a blurred intensity distribution of a real object after being convolved with the PSF. Due to the finite width of the PSF of *Yohkoh* SXT, a certain amount of blurring effect has been expected in the observed images. Especially for flaring regions, it is necessary to remove these blurred components for both morphological and photometric purposes. Therefore, for restoring true intensity distributions from observed SXT images, it is necessary to understand in advance the detailed information on the PSF.

The SXT is a grazing-incidence mirror telescope having a 1024×1024 pixel CCD detector as a recording device of X-ray images. A couple of ground experiments had been carried out for the calibration of the SXT mirror prior to launching the satellite. The initial calibration performed using the 1000 foot X-ray calibration facility at Marshall Space Flight Center (MSFC) revealed that the SXT mirror, fabricated with both elements on a single substrate of Zerodur, has excellent imaging properties with low scattering. A gold coated hyperboloidal figure of each mirror (Nariai 1987, 1988) gives better off-axis imaging performance than a Wolter-I mirror, although at an expense of on-axis resolution. The test techniques and results have been published by Lemen et al. (1989). Tsuneta et al. (1991) has first introduced the general feature of the SXT PSF in detail. According to the paper, the PSF has a very sharp peak, and the wings have non-Gaussian profiles. Also they showed that the PSF has a much improved low scattering level compared to the *Skylab S-054* telescope (Vaiana et al. 1977). Later we have known the details of the scattering characteristics of the SXT mirror from in-flight data analysis (Hara et al. 1994) that the far wings of the SXT PSF fall off as the inverse square of the distance from a bright image feature beyond about 20 arcsec. One of the common means characterizing the PSF is the full width at half maximum (FWHM) of the best fit functional form. For the SXT, the FWHM of the on-axis PSF is revealed more or less than one pixel size (~2.46 arcsec). Tsuneta et al. (1991) also showed in their figure that the FWHM varies along the distance from the optical axis.

The final calibration of the SXT mirror was carried

Corresponding Author: J. Shin

out at White Sands Missile Range (WSMR) in April 1991, only four months prior to the launch of *Yohkoh*. This experiment has an important meaning that all the SXT configuration was given for the first time in an in-flight state except for the X-ray filters. Martens et al. (1995) measured the SXT PSF by fitting an elliptically modified Moffat function (Moffat 1969) to this experiment data in Fourier space. It is known from their results that the PSF of WSMR is slightly broader than the previous result. Also the degree of off-axis variation of the PSF was reduced in comparison with the result obtained using the MSFC data. They were thought reasonable because in the in-flight state the CCD has been set 0.1 mm forward of the position of best focus of the SXT (Lemen et al. 1989), in order to provide a more uniform angular resolution across the 42 arcmin field-of-view of the telescope. What should be pointed out in their study, however, is that most of the results showed very large deviations. For example, even for the results obtained at an identical location on the CCD, the dispersion in fitting parameters was too large to define a certain PSF, which implies that their method for finding the best fit function might not be suitable for the SXT PSF. Also, these large errors in the fitting made it difficult to understand the off-axis variations of the PSF at each wavelength. For these reasons, the best fit functions for the SXT PSF derived by Martens et al. (1995) seem to be inappropriate for explaining optical characteristics of the SXT mirror, hence for removing correctly the blurred components from the observed images. Therefore, we have decided to re-analyze the pre-launch calibration data of SXT mirror and measured the shape of the PSF. In the next section, we will suggest several reasons why the SXT PSF could not be determined properly when normal fitting methods were applied to the calibration data.

II. METHOD OF ANALYSIS

(a) The Elliptical Moffat Function

It has been expected from the previous studies that the SXT PSF has a sharp peak at the core and comparatively broad wings. Besides, the contours of the WSMR measurements appear elliptical near the edges of the CCD. Thus we have adopted in our study a Moffat function, which is elliptically modified for finding the best fit functional form of the SXT PSF. Details on the elliptical Moffat function is described in Martens et al. (1995): For a rotationally symmetric Moffat function, an intensity at a location (x, y) on the focal plane can be expressed as follows :

$$PSF(x,y) = c \times \left[1 + (r/a)^2\right]^{-b} \qquad (1)$$

where a and b are the primary parameters for the fit and x and y are the coordinates of the function, expressed in pixel units. These parameters are responsible for the form of the Moffat function, while c measures only the peak photon count, which is proportional to the exposure time. Thus, the distance from the peak of the PSF to the location (x, y) is $r^2 = x^2 + y^2$. For considering the ellipticity of the Moffat function, r should be modified such as

$$r^2 = x^2 + y^2 + e\Big[x^2\{1 + \cos 2\phi\} + y^2\{1 - \cos 2\phi\} + 2xy \sin 2\phi\Big] \qquad (2)$$

where e is an ellipticity of the Moffat function and ϕ is an angle between the x axis and the major axis of the ellipse in counterclockwise direction. The constant c will be determined from the normalization condition,

$$\int_{-\infty}^{\infty}\int_{-\infty}^{\infty} PSF(x,y)dxdy = 1. \qquad (3)$$

These five Moffat parameters will be determined from the fitting of the model function to the ground experiment data.

(b) The Undersampling Effect

The FWHM of the SXT PSF is only about one pixel size and the intensity drops very fast as it goes away from the peak, Thus the core of the PSF consists of only a small number of pixels, which implies the SXT data will be undersampled during the observation. This undersampling effect is also clearly seen from the ground experiment data. In general, the profile of the undersampled PSF core is asymmetric, and cannot be described precisely with only a few pixels. Therefore, for evaluating the best fit of the PSF, it is thought crucial to consider carefully the undersampling effect.

Martens et al. (1995) considered the undersampling by slightly shifting the original Moffat function: They adopted the method of direct fitting of a model Moffat function to the measured values of data. For simplicity, let us use a one-dimensional model for illustration. Each CCD pixel is labeled by an integer, t, and the location of pixel having maximum X-ray intensity is represented by x_m. Thus the CCD pixel at t will have a relative coordinate, $x = x_t - x_m$, in unit of the pixel size. Then, for the case when the data is severely undersampled, the real peak of the model Moffat function will not always be located exactly at the center of the pixel. Thus the offset of the peak with regard to the center of the peak pixel should be considered properly. When the offset is assumed as x_o, the CCD pixel at t will have a coordinate, $x = x_t - x_m - x_o$, and finally the intensity of a pixel at x will be described by the function,

$$I(x) = PSF(x_t - x_m - x_o). \qquad (4)$$

However, it is revealed from our study that this kind of method is not enough to consider the undersampling

effect satisfactorily. We have performed a numerical simulation using a model PSF for finding the problems in their method. Figure 1 shows the results of fitting for different locations of peaks in the maximum pixel. It is apparent from the figures that, especially when the peak is located at the center of the pixel (Figure 1a), the intensity at the maximum pixel will always be severely underestimated. It is interesting that the degree of underestimation becomes smaller as the PSF peak goes away from the center of maximum pixel. When the peak is located near the edge of the pixel, the accuracy of fitting comes to a maximum. What should be noted here is that the results depend sensitively upon the location of the peak inside the maximum pixel, which means that we will not be able to derive a correct answer from the fitting, even for the case we know the exact location of the peak.

For the purpose of considering the undersampling effect properly during the fitting of the model PSF function, we have developed a method of subpixelization of CCD pixels: The measured PSFs are the functions represented by CCD pixels, while the Moffat function is a continuous analytical function. Thus the comparison between the measured PSFs and the Moffat function should be made after sampling the Moffat function once in every pixel. To solve this problem, we reconstruct a true PSF with a finer grid, which are obtained by dividing each CCD pixel into $2N+1$ subpixels (in one-dimensional model), where N is an integer, such that the total number of subpixels should be odd for mathematical convenience. The larger the number of the subpixels considered, the closer the form of the reconstructed PSF to that of analytical function. The subpixels are labeled by an integer, i, so that the center of the subpixel at i has a Cartesian coordinate $x_i = i/(2N+1)$, where $-N \leq i \leq N$. As a consequence, the blurred intensity projected onto the CCD pixel at x will be given by

$$I(x) = \frac{1}{2N+1} \sum_{i=-N}^{N} PSF(x - x_i)$$
$$= \frac{1}{2N+1} \sum_{i=-N}^{N} PSF(x_t - x_m - x_o - x_i) \quad (5)$$

where PSF is the Moffat function of subpixels before being undersampled.

Figure 2 shows the result when our subpixelization method is applied. It is clear from the figures that, regardless of the location of the peak inside the maximum pixel, our method successfully reproduces the model function. Obviously, the smaller size of subpixels will suggest the more accurate result of fitting. In this study, for saving calculation time, we limited the degree of subpixelization such that a size of total 21×21 subpixels becomes equivalent to the size of the SXT CCD pixel. Simulation has proved that the degree of subpixelization adopted is enough to find the best fit

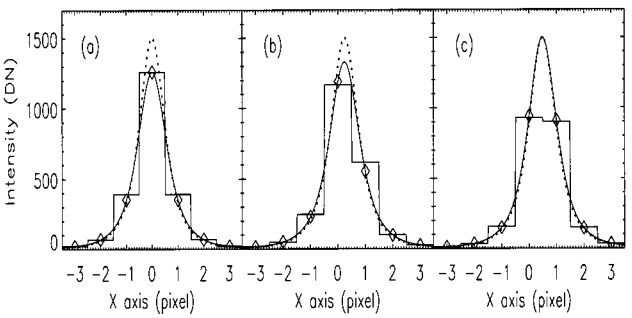

Fig. 1.— Numerical simulation for the evaluation of the best fit one-dimensional PSF profile by fitting each pixel point with a Moffat functional form. Undersampling effect is considered only by estimating the degree of offset of the peak position inside the maximum pixel: (a) when the peak is at the center of the maximum pixel, (b) when the peak is about a quarter of the pixel size apart from the center and (c) when the peak is located near the edge of the pixel.

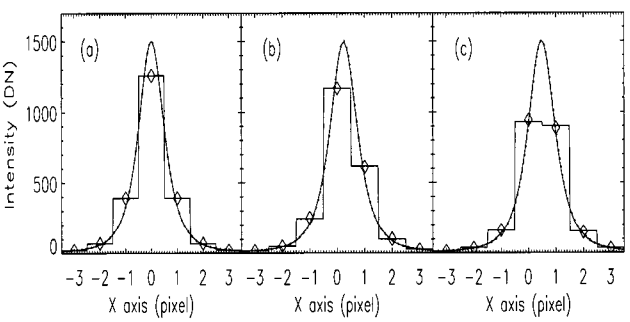

Fig. 2.— Same as Figure 1 but for the application of the method of subpixelization in this study.

model of the SXT PSF with high accuracy for both coefficients a and b.

(c) Fitting Procedure

The aim of this study is to determine the SXT PSF by deriving the best fit analytical relation among the noisy quantities obtained from the ground experiment. One of the most widely used and best understood tool for carrying out this kind of analysis is the so-called "chi square minimization" method. This has been known as a very powerful technique and useful in a wide variety of data reductions. Generally, the goodness-of-fit between observed data values of $I_{\rm obs}$, with errors, σ, and an expected model, $I_{\rm exp}$, can be determined by using the standard χ^2 statistic:

$$\chi^2 = \sum_x \sum_y \frac{[I_{\rm obs}(x,y) - I_{\rm exp}(x,y)]^2}{\sigma^2(x,y)} \quad (6)$$

where (x, y) means the position of each pixel on the CCD. In most experiments, however, we do not know

what the values of σ are, in case we make only one set of measurements. Fortunately, by assuming Poisson statistics, these uncertainties can be estimated from the data directly without measuring them explicitly. For the Poisson distribution, the variance σ^2 is known to be equal to the mean of the distribution (Bevington 1969). It is common to assume that the errors follow the Poisson distribution. Thus, for Poisson-distributed data, Equation (1) can be expressed using Pearson's chi square statistic (Pearson 1900):

$$\chi^2 = \sum_x \sum_y \frac{[I_{\rm obs}(x,y) - I_{\rm exp}(x,y)]^2}{I_{\rm exp}(x,y)}. \quad (7)$$

For the calibration using the chi square minimization method, the digital signals of the calibration data need to be turned back into photon counts. The CCD of the *Yohkoh* SXT measures the number of free electrons produced by X-ray photons in each pixel. And then the analog result is divided by the gain factor, g, which is a constant set to prevent saturation in the 12-bit A/D converter. For the WSMR tests the gain factor is known as 100, and in orbit approximately 90 to 100. This yields the unit of observed SXT images, the so-called Data Number (DN). Since the energy of one photon is $1.24 \times 10^4/\lambda\ eV$, where λ is the photon wavelength in Å, and it requires 3.65 eV to produce an electron-hole pair in silicon, 3.65 times the number of produced electrons becomes equivalent to the total energy of photon counts, I. Thus, the photon count I can be obtained directly from the digital signal, DN :

$$I = 2.94 \times 10^{-4} \cdot \lambda \cdot g \cdot DN. \quad (8)$$

However, it is revealed in our study that this chi square statistic is not suitable for finding the best fit functional form of the SXT PSF. It is because the result for chi square statistic depends strongly upon the size of the image considered. In this paper we will report using the numerical simulation the size dependence of the result when the chi square statistic is applied. Figure 3 shows the simulated results of the size dependence of the best fit Moffat function. The chi square value of each model is set not so much deviated from unity. As the size of the image increases, both the Moffat coefficients a and b become gradually deviate from the true solutions, which must be related to the low photon counts of pixels far from the peak. However, as is seen from the figure, merely reducing the size of the image would not be helpful because it will instead increase the uncertainty in the result due to insufficient sample pixels.

Simulations have shown that applying the chi square statistic is not appropriate for deriving the best fit functional form from the experiment data of *Yohkoh* SXT because the pixels far from the PSF peak have in general low photon counts. It has been known for decades by the scientists that the chi square method is no longer applicable when there are only small numbers of photon counts per pixel. Cash (1979) demonstrated that a maximum likelihood estimator based on the Poisson probability distribution can be used to derive best fits. The so-called Cash's C statistic is derived by taking the logarithm of the likelihood function, changing its sign, dropping the factorial term, and multiplying by two:

$$C = 2 \sum_x \sum_y \Big[I_{exp}(x,y) - I_{obs}(x,y) \cdot \ln I_{exp}(x,y) \Big]. \quad (9)$$

Minimizing C for some model gives the unbiased best fit parameters.

Figure 4 shows the results of simulation using C statistic. It is revealed from the figures that the Moffat coefficients no longer have size dependences, regardless of the assumed total intensity. In conclusion, we have adopted in our study the C statistic for finding the best fit elliptical Moffat function as a model of the SXT PSF. It is noted, however, as was the same for the case of chi square statistic, we cannot avoid large deviation among the results in the case of low total intensity. A simple solution of this problem would be to fit the observed data as many as possible and take a mean of the coefficients.

(d) Location of the Optical Center

The PSF is a function of the off-axis angle. In order to examine the variation of the PSF in a field-of-view, it is necessary to define in advance the location of the optical axis on the CCD. For a perfect mirror the optical axis is a longitudinal line that defines the central axis of the annular X-ray mirror. Knowledge on the optical axis is mainly needed to determine the optical characteristics of the telescope as a function of off-axis angle as well as photon energy. Not only the PSF but also the effective area of the mirror is a function of off-axis angle within the field-of-view. With increasing off-axis angle, less of the photons entering the telescopes actually reach the focal plane. This effect is called 'vignetting'.

The vignetting of the SXT, which is reflected by the decline of the telescope's effective area as a function of off-axis angle, has been studied thoroughly by the *Yohkoh* scientists. The effective area and response functions that are reported in the papers always refer to the values for the optical axis of the telescope, where the effective area is maximum. The off-axis response has been measured during the pre-launch calibrations and has been refined with in-flight data analysis. To a first approximation, the off-axis variation of effective area, or the vignetting function, was approximated by two non-concentric cones (Fuller et al. 1994). The inner region is the part of the axial response curve that is due to the mirror's X-ray characteristics. The outer region is the part of the combination of the effects due to the mirror's response and due to internal occultation (called

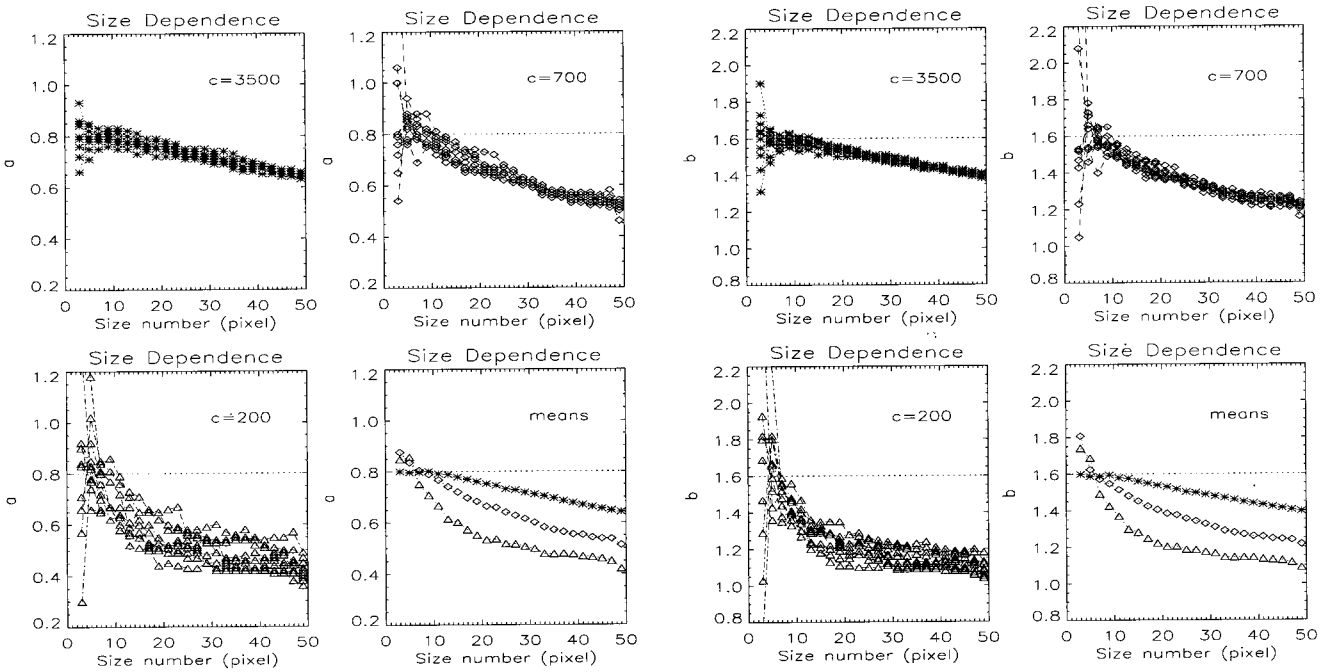

Fig. 3.— Simulations for evaluating the size dependence of the best fit Moffat function. Rotationally symmetric Moffat function whose coefficients $(a, b) = (0.8, 1.6)$ has been used as a model PSF. A total of ten images to which random Poisson noise has been added are produced for the simulation. Chi square statistic has been applied for finding the best fit functional form of each noisy image. The first three figures of each a and b pair show variations for different values of c. Finally the size dependences of the average of coefficients for each c are plotted for comparison (asterisks: c=3500, diamonds: c=700 and triangles: c=200, respectively). The size number, M, is an integer such that $2M+3$ equals the total number of pixels in the image considered.

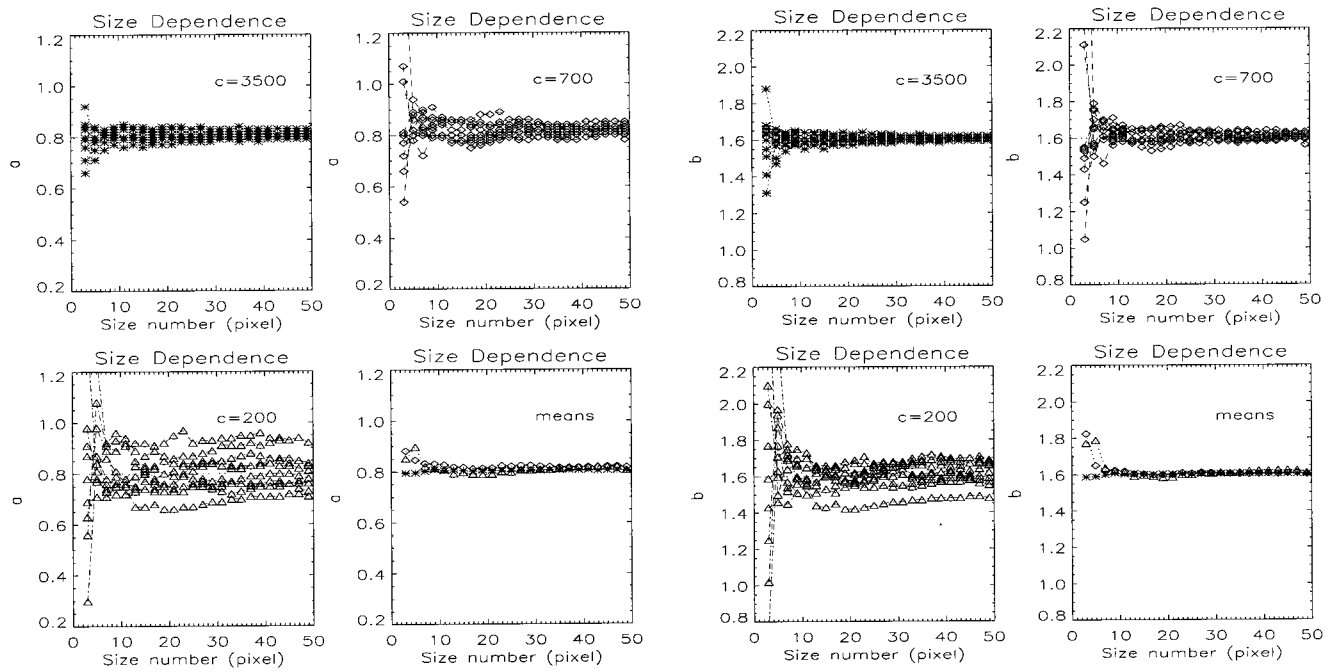

Fig. 4.— Same as Figure 3 except for the application of C statistic.

vignetting effect). The inner- and outer-cones intersect one another at a radius of about 21 arcmin. Later, analysis of in-flight data indicated that the vignetting function is actually more complicated and should be approximated by a cone with some flat distortions, which were not detected during the pre-launch calibrations. There are, however, no fully approved methods to remove or correct for the SXT vignette function. In this study, we will examine the variation of the effective area of the SXT mirror using the pre-launch experiment data of WSMR and the simulations, and discuss the problems in determining the optical center.

The vignetting function is known to vary as a function of incident photon energy. Pre-launch measurements at WSMR were made at three energies: 0.277 KeV (C-K), 1.49 KeV (Al-K) and 2.98 KeV (Ag-L). Since the measurements at two lower energies gave results that were consistent with one another, *Yohkoh* scientists have characterized the SXT vignetting functions as either low or high energy. The SXT was pointed to various off-axis positions and the signal was recorded using the CCD. The facility had a proportional counter which continuously monitored the X-ray photon flux, F_i, incident on the telescope. Knowing the geometric area, A, the effective area was determined from the equation, $A_e = (F_d \times A)/F_i$, where F_d is the photon flux measured on the focal plane. Since an analysis of the proportional counter data showed that the variations in the incident beam were less than one sigma, the incident X-ray flux is considered to be constant over the field-of-view. Therefore, we will examine the vignetting effect of the SXT using the variation of the photon flux, F_d, which was obtained by binning the 11×11 core pixels of each PSF image.

Figure 5 shows the vignetting effect of SXT at each wavelength. Figure 5a is the response function centered on the location of the optical axis obtained from the inner region data. For low energies, compared to the inner region, the distribution at the outer region shows a poor correlation. It is thought that this has made the scientists consider two non-concentric cones for explaining the SXT vignetting effect. By considering another optical center, they attempted to reduce the dispersion in the outer region of the field-of-view (Figure 5b). Now we ask a question whether the concept of two different optical centers is inevitable for the explanation of this peculiar pattern of the SXT vignetting function. We have found an interesting fact that the data obtained near the upper edge of the CCD were always located at the lower part of the distribution (crosses in Figure 5). And when we omit these points from the figure, the rest of the points show a smooth distribution with good correlation (Figure 5c). Therefore, we understand that the concept of two non-concentric cones is only for reducing the dispersion by the data obtained at a certain region on the CCD.

However, it is obvious that simply ignoring these points cannot be an answer for the vignetting effect of SXT. We have revealed using the simulations that the

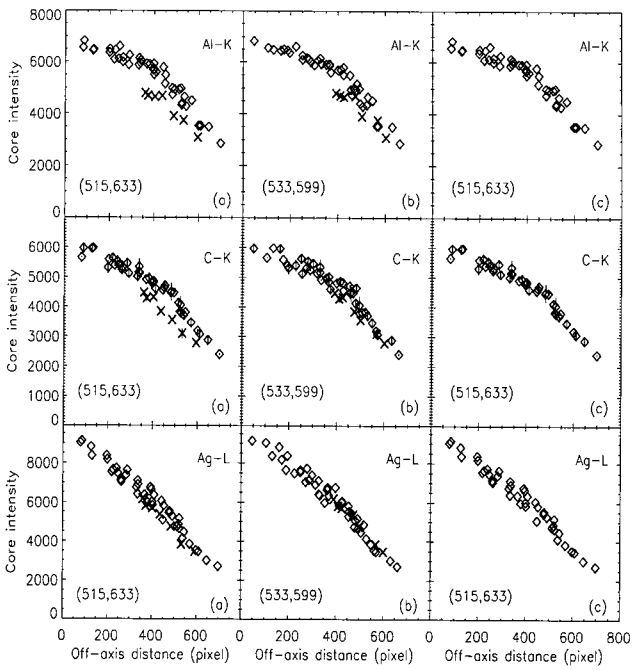

Fig. 5.— Vignetting effect of SXT for different energies. Symbols indicate the photon flux at each location on the CCD. Among them, the crosses are for the data obtained near the upper edge of the CCD: (a) when the location of the optical center on the CCD is assumed as (515,633), (b) when the location of the optical center on the CCD is assumed as (533,599), (c) same as (a) but the cross symbols has been omitted.

peculiar characteristics of the SXT vignetting function is due to the offset of the optical axis from the geometrical center of the telescope. Let us first assume original response functions (Figure 6a) for low and high energies, which are due to the mirror's X-ray characteristics. Their distributions are given as symmetric with respect to the optical axis. The response function will be degraded at the outer region of the field-of-view by the internal occultation. We assume the degree of internal occultation (Figure 6b), by which the original response functions are degraded. It is noted that the internal occultation should be defined according to the distance from the geometrical center. Then the final function of the vignetting will be a combination of the effects due to the original response and the internal occultation. When the optical axis is located exactly on the geometrical center, as is seen in Figure 6c, the vignetting functions will be described with simple curves. However, as was expected for the case of SXT, when either of x (or y) coordinate of the optical axis deviates from the geometrical center, the vignetting function becomes broader, especially at the outer region (Figure 6d), and the degree of broadening is severer for low energy. In Figure 6e, we plot the values of photon flux at the same positions where the WSMR data were obtained. The seven points (rectangles) in Figure 6e,

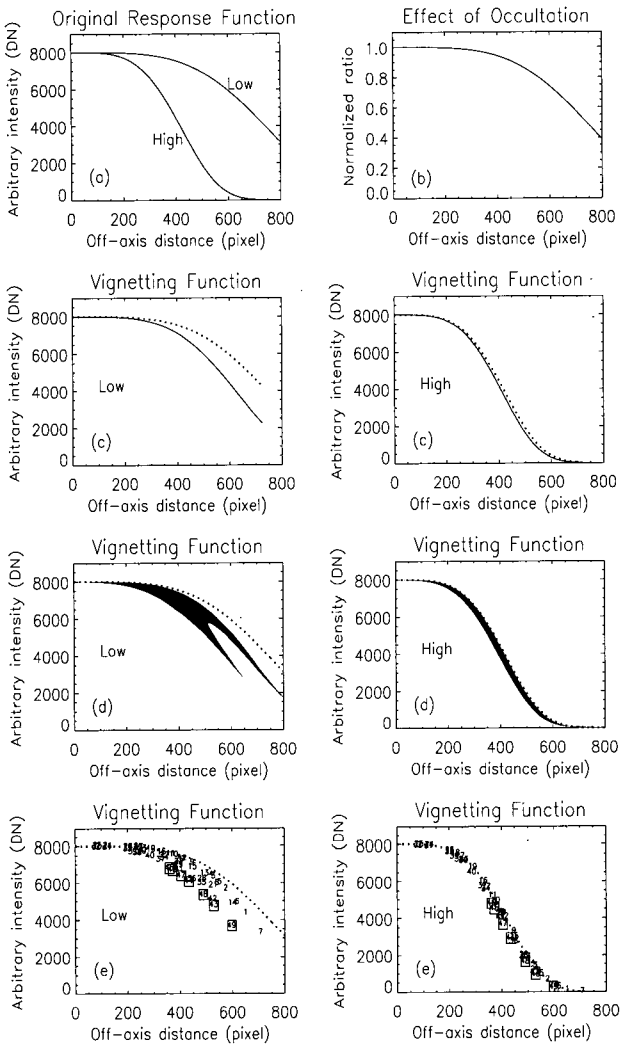

Fig. 6.— Simulation of vignetting effect for various cases of the location of optical center. Dotted lines are the original response functions for both low and high energies. Details on each figure are written in the text.

which are obtained near the upper edge of the CCD, are always located at the lower part of the distribution. We have already seen these phenomena from the real vignetting functions of SXT in Figure 5. Also it is interesting that, compared to low energies, the effect by the internal occultation seems smaller for high energy. It is because the original response function of high energy drops faster, hence being less affected by the effect of occultation (Figure 6d).

As a conclusion, it is believed that the peculiar pattern of the vignetting effect of SXT can be explained by the offset of the optical axis from the geometrical center. However, there remains a problem of how to determine the location of the optical center using the pre-launch data. Therefore, for the determination of the exact location of optical axis, it is necessary to

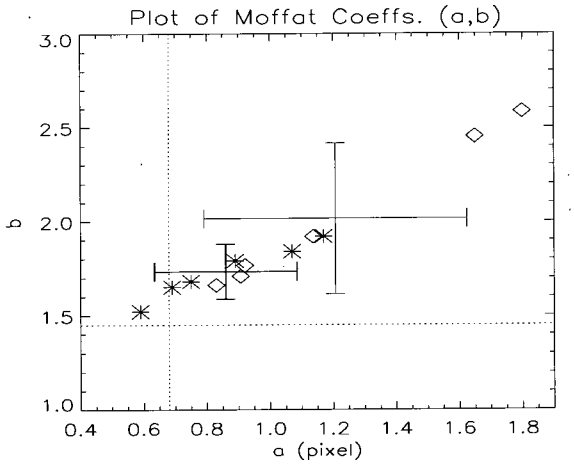

Fig. 7.— Best elliptical Moffat fits for six WSMR data obtained at an identical location near the optical center. Diamonds are the results of Martens et al. (1995), and asterisks are from our study. The thin and thick lines indicate the locations of the mean values and the error ranges for two results, respectively. Dotted lines are the average of (a, b) for all the Al-K data of WSMR presented by Martens et al. (1995).

study more thoroughly the vignetting effect of SXT.

III. RESULTS AND DISCUSSION

Using the methods presented in the previous section, we have analyzed the pre-launch calibration data of WSMR and evaluated the best fit elliptical Moffat function for the SXT PSF. Figure 7 shows the results of best elliptical Moffat fits for six images in the file, *bx19_apr24*, obtained at a region near the optical center. We see from this figure that the results of Martens et al. (1995) show large deviation. Besides, it should be pointed out that the mean of these six PSFs differs considerably from the average of all the Al-K data used in their study. This kind of inconsistency implies that the results of best fit function for the SXT PSF derived by Martens et al. (1995) are not appropriate for explaining optical characteristics of the SXT mirror. Compared to the results of Martens et al. (1995), ours show the deviation remarkably reduced. The average of our results for six PSFs lies between the two results of Martens et al. (1995) in the figure. We cannot expect, however, which one of their results will be closer to an answer, because as we have explained in the previous section there are several possibilities which can make the PSF over- or underestimated.

Figure 8 shows the off-axis variation of the SXT PSF for C-K data. It is very important to understand this spatial variation of the PSF because coronal activities happen on the limb as well as on the disk center. We have found the FWHM of the PSF stays nearly constant within the error bound up to about 400 pixel

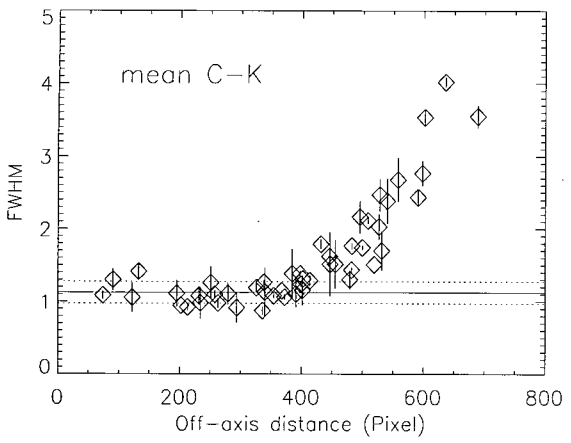

Fig. 8.— Off-axis dependence of the SXT PSF for C-K line (44.7 Å) data. The result is an average of two data sets, *bx42_apr25* and *bx51_apr25*, which were obtained at different exposure times, respectively. The error bar shows the difference of two results at each location. The solid and dotted lines are the mean and the standard deviation of the data inside the 400 pixel distance, respectively.

distance from the optical center. Beyond this distance, it begins to increase gradually. From this result, it is expected the degree of blurring will be almost the same over the central area of the CCD where the solar disk is located. We could explain the detailed variation of the PSF on the solar disk, as has been expected for Wolter-I type mirror (Nariai 1987, 1988). In this paper, however, we will not argue about the minor variation of the SXT PSF on the region of solar disk, because we still have some unsolved problems, *e.g.*, the location of the optical axis on the CCD.

In comparison with the data near the optical center, the results at the outer region of the field-of-view seem to have larger dispersion. It could be because, with increasing off-axis distance, less photons entering the telescopes will arrive at the focal plane due to the vignetting effect. We have known from the simulation that the dispersion of the best fit functions increases as the total intensity of the image decreases (Figure 4).

It is revealed from our analysis that the FWHM of the SXT PSF for high energy is slightly broader than that for low energies, though the difference was not so large. What has been concerned so far in this paper is the shape of only the core part of the SXT PSF. For a complete characterization of the SXT PSF, the scattering wing component should be connected smoothly to the core. According to Hara et al. (1994), the far wings of the PSF fall off as the inverse square of the distance beyond about 20 arcsec. And the level of the scattering wings will apparently be higher for the shorter wavelength. As a result, it is possible that a portion of scattered component has been added to the core of the PSF for high energy. Spectral consideration will be a future study for featuring a complete form of the SXT PSF from the core to the scattering wing.

More detailed description on the SXT PSF will appear soon in *Solar Physics*.

REFERENCES

Bevington, P. R. 1969, Data Reduction and Error Analysis for the Physical Sciences, McGraw-Hill, New York

Cash, W. 1979, Parameter Estimation in Astronomy through Application of the Likelihood Ratio, ApJ, 228, 939

Fuller, R. A., Lemen, J. R. & Acton, L. W. 1994, SXT X-Ray Vignetting Function, SXT Calibration Note 37

Hara, H., Tsuneta, S., Acton, L. W., Bruner, M. E., Lemen, J. R., & Ogawara, Y. 1994, Temperatures of Coronal Holes Observed with the Yohkoh SXT, PASJ, 46, 493

Lemen, J. R., Clafin, E. S., Brown, W. A., Bruner, M. E., Catura, R. C. and Morrison, M. D. 1989, Measurement of the Point Spread Function and Effective Area of the Solar-A Soft X-Ray Telescope Mirror, SPIE, 1160, 316

Martens, P. C., Acton, L. W. & Lemen, J. R. 1995, The Point Spread Function of the Soft X-Ray Telescope aboard Yohkoh, Sol. Phys., 157, 141

Moffat, A. F. J. 1969, A Theoretical Investigation of Focal Stellar Images in the Photographic Emulsion and Application to Photographic Photometry, A&Ap, 3, 455

Nariai, K. 1987, Geometrical Aberration of a Generalized Wolter Type I Telescope, Appl. Opt., 26, 4428

Nariai, K. 1988, Geometrical Aberration of a Generalized Wolter Type I Telescope. 2: Analytical Study, Appl. Opt., 27, 345

Ogawara, Y., Takano, T., Kato, T., Kosugi, T., Tsuneta, S., Watanabe, T., Kondo, I. & Uchida, Y. 1991, The Solar-A Mission: An Overview, Sol. Phys., 136, 1

Pearson, K. 1900, On a criterion that a given system of deviations from the probable in the case of a correlated system of variables is such that it can reasonably be supposed to have arisen from random sampling, Philos. Mag., Set 5, 50, 157

Tsuneta, S., Acton, L., Bruner, M., Lemen, J., Brown, W., Caravalho, R., Catura, R., Freeland, S., Jurcevich, B., Morrison, M., Ogawara, Y., Hirayama, T. & Owens, J. 1991, The Soft X-ray Telescope for the Solar-A Mission, Sol. Phys., 136, 37

Vaiana, G. S., Van Speybroeck, L. P., Zombeck, M. V., Krieger, A. S., Silk, J. K., & Timothy, A. F. 1977, The S-054 X-ray telescope experiment on SKYLAB, Space Sci. Instrum., 3, 19